scientific reports

Check for updates

OPEN

Bidirectional multi-nodes quantum teleportation using discrete-time quantum walk

N. Ikken[1], P. Kumar[2], A. Slaoui[1,3,4]✉, B. Kar[2], R. Ahl Laamara[1,3], M. Zomorodi[5] & A. A. Abd El-Latif[4,6]

We suggest a new technique for bidirectional quantum teleportation (BQT) that combines coherent-state encoding with discrete-time quantum walks to allow two users to communicate quantum information simultaneously. Our method enables Alice and Bob to simultaneously teleport quantum states to one another within a single protocol, as compared to unidirectional teleportation, which only transmits quantum states in one direction. To allow for a qubit-like representation and fidelity analysis using Bloch vector formalism, the quantum information is encoded using non-orthogonal coherent states that are converted into an orthonormal basis of even and odd Schrödinger cat states. Four different quantum walk steps, each acting on a three-part quantum system made up of position and coin spaces, drive the teleportation process. We use density matrix overlaps in the even–odd basis to derive closed-form formulas for teleportation fidelity in both directions analytically. Using the SeQUeNCe discrete-event simulator, we simulate large-scale quantum network settings with realistic limitations, including photon loss, memory decoherence, entanglement swapping degradation, and various channel capacities in order to evaluate the potential of our approach. We evaluate quantum memory utilization, throughput, and end-to-end fidelity in various network topologies and scenarios. Our findings demonstrate that BQT allows symmetric communication with strong fidelity, particularly in high-capacity and large-scale network situations, but requires a greater resource overhead than unidirectional protocols. The hybrid framework developed in this study offers a scalable and analytically simple solution for next-generation quantum communication systems by combining discrete-time quantum evolution with continuous-variable state encoding.

Keywords Bidirectional quantum teleportation, Discrete-time quantum walks, Coherent states, Quantum network simulation, Bloch sphere fidelity, SeQUeNCe

One of the most well-known methods in quantum information theory is quantum teleportation, which provides a way to move unknown quantum states between different places without actually sending the particles. Teleportation was first introduced by Bennett and associates in the early 1990s[1], and since then, it has been a fundamental component of distributed quantum computation, quantum cryptography, and quantum communication[2–6]. Recent developments have sparked an increasing interest in *Bidirectional Quantum Teleportation* (BQT)[7,8], where two users concurrently exchange quantum information, while the majority of early implementations and theoretical models were on *Unidirectional Quantum Teleportation* (UQT). In addition to improving channel efficiency, this symmetric communication style satisfies the structural requirements of scalable quantum networks[9,10]. But the fundamental entanglement distribution process's scalability and stability provide an important obstacle to teleportation. Inspired by the classic idea of random walks, discrete-time quantum walks (DTQWs)[11] have become effective tools for resembling quantum dynamics and allowing intricate quantum network protocols. Contrary to their classical equivalents, DTQWs take advantage of quantum interference and superposition to achieve richer dynamics and faster transmission. DTQWs are everywhere for

[1]LPHE-Modeling and Simulation, Faculty of Sciences, Mohammed V University in Rabat, Rabat, Morocco. [2]Department of Computer Science and Information Engineering, National Taiwan University of Science and Technology, Taipei, Taiwan. [3]Centre of Physics and Mathematics, CPM, Faculty of Sciences, Mohammed V University in Rabat, Rabat, Morocco. [4]EIAS Data Science Lab, College of Computer and Information Sciences, and Center of Excellence in Quantum and Intelligent Computing, Prince Sultan University, 11586 Riyadh, Saudi Arabia. [5]Department of Computer Science, Faculty of Computer Science and Telecommunications, Cracow University of Technology, Kraków, Poland. [6]Jadara University Research Center, Jadara University, Jordan, Jordan. ✉email: abdallah.slaoui@um5s.net.ma

quantum computation and helpful for building quantum search and routing algorithms, according to theoretical studies[12–14]. These features make them particularly well-suited for controlling the propagation of states in a teleportation protocol that necessitates coherence within various subsystems.

We use DTQWs' transport capabilities in our suggested scheme to create a reliable and effective bidirectional teleportation mechanism[15]. We base our approach on a new framework in which the teleportable information is represented in superpositions of non-orthogonal coherent states rather than qubit states. Often used in quantum optics, coherent states are more appropriate for continuous-variable quantum communication systems and are naturally resilient to some forms of noise[16]. We express the incoming quantum information in a discrete, qubit-like form by building an orthonormal basis of even and odd coherent states, also referred to as Schrödinger cat states[17,18]. This makes processing and fidelity analysis easier.

We can use Bloch vector formalism to analytically model the teleportation process by encoding Alice's and Bob's states in such a basis. By using this formalism, we may represent the input and output quantum states as density matrices with directional vectors and transfer them to locations on the Bloch sphere[19]. In addition to offering a clear geometric representation of the protocol, this method makes it possible to precisely calculate the fidelity of teleportation, a measure of how closely the transmitted state matches the original.

Four discrete-time quantum walk steps are used to carry out the actual teleportation procedure. Alice and Bob, each have a three-part system that includes two coin spaces and a position. These systems are set up so that one of the coin registers corresponds to the unknown quantum state of each user. The quantum walk's steps are made to apply Hadamard gates and conditional shift operations, ensuring the logical development and final exchange of encoded quantum information[20]. The simultaneous bidirectional quantum teleportation is made possible throughout the evolution by interference effects brought about by quantum superposition.

We used the SeQUeNCe quantum network simulator[21] to perform a thorough evaluation of performance in order to determine the possibility of the suggested system. Realistic quantum communication networks with physical limitations, including decoherence, photon loss, channel attenuation, and memory limits, are modeled by this simulator. We examine the performance, fidelity, and quantum memory utilization of the teleportation protocol in our simulation scenario, which is a 200 node network with Waxman connections[22]. The results show that BQT provides competitive fidelity and network utilization in exchange for its symmetric and concurrent communication capacity, even though it fundamentally uses more resources than UQT.

In addition, we find that coherent-state encoding improves resilience against noise and loss, which are particularly damaging in long-distance quantum communication[23], in addition to providing a deeper framework for quantum state representation. The suggested protocol exhibits potential for practical applications of symmetrical quantum communication lines and next-generation quantum internet infrastructure when paired with DTQW-based routing and entanglement distribution[24,25].

Finally, we present an adaptable and analytically simple model for bidirectional quantum teleportation that combines coherent-state encoding with discrete-time quantum walks. Through the integration of ideas from discrete quantum computation and continuous-variable quantum optics[26], we develop a hybrid teleportation framework that is compatible with the real-world limitations of large-scale quantum networks while ensuring high-fidelity transmission. Therefore, the suggested approach provides opportunities for further study of fault-tolerant entanglement routing strategies, adapted quantum walks, and hybrid CV-DV teleportation schemes[27].

Related work

Bennett et al.[1] were the first to introduce quantum teleportation, which laid the foundation for non-local quantum communication through the use of shared entanglement and classical channels. Unidirectional quantum teleportation (UQT), in which quantum states are transferred from a sender to a receiver in a single direction, was the main focus of early research. Since then, these protocols have been extended into higher-dimensional and multi-qubit frameworks[20].

A symmetric variant of UQT that allows two users to exchange quantum states at the same time is called bidirectional quantum teleportation (BQT). Numerous models have been developed in this direction, such as hybrid techniques using discrete and continuous variables[8,27], and controlled bidirectional teleportation using multi-qubit entangled states[7,28]. Additionally, in[29], the theoretical framework for general quantum networks was built.

Discrete-time quantum walks (DTQWs) have become a promising tool in quantum communication and computation in recent years. The algorithmic applications of DTQWs[30,31], fast state propagation, and interference-based benefits over conventional random walks[32] have all been the subject of much research. Because of these characteristics, they are especially appropriate for tasks like teleportation[33] that require coherent quantum state transfer.

Through DTQW dynamics, teleportation has been explored in several attempts. Krishna et al.[33], for example, used quantum walks on particular graph configurations to study bidirectional teleportation. However, a lot of models have ignored the useful advantages of continuous-variable systems in favor of concentrating on qubit-based encoding.

Coherent-state teleportation techniques have been investigated for their noise resistance and feasibility in optical networks in the field of continuous-variable quantum communication[34–36]. As proven by Ikken et al.[8], recent work has suggested encoding qubit-like information in non-orthogonal coherent states and analyzing them in orthonormal cat-state bases.

As far as we are aware, our suggested protocol is the first to combine a complete bidirectional quantum walk-based teleportation framework over multi-node quantum networks with coherent-state encoding. Additionally, we offer performance simulations under realistic limits using SeQUeNCe[21] as well as analytical fidelity derivations applying Bloch vector formalism. In addition to showing excellent fidelity, this hybrid CV-DV method provides flexibility and scalability for designing quantum networks.

One-dimensional quantum walk

A one-dimensional discrete-time quantum walk[37] takes place in the composite Hilbert space

$$\mathcal{H} \;=\; \mathcal{H}_P \otimes \mathcal{H}_C, \tag{1}$$

where

$$\mathcal{H}_P = \text{span}\{\,|n\rangle : n \in \mathbb{Z}\}, \qquad \mathcal{H}_C = \text{span}\{\,|0\rangle,\; |1\rangle\}.$$

Here, $\mathcal{H}_P$ represents the infinite one-dimensional lattice of positions labeled by integer n, and $\mathcal{H}_C$ is a two-dimensional "coin" space that governs the direction of motion.

State of the walker

At discrete time t, the full state of the walker is[38]:

$$|\Psi(t)\rangle \;=\; \sum_{n\in\mathbb{Z}} \left[\psi_{n,0}(t)\,|n\rangle\otimes|0\rangle \;+\; \psi_{n,1}(t)\,|n\rangle\otimes|1\rangle\right] \tag{2}$$

where $\psi_{n,c}(t) \in \mathbb{C}$ and $\sum_{n,c} |\psi_{n,c}(t)|^2 = 1$.

Single-step evolution

One time-step of the walk is implemented by the unitary operator[39]

$$W(\ell) \;=\; E(\ell)\;(I \otimes C)\,, \tag{3}$$

where C is the *coin operator* acting on $\mathcal{H}_C$:

$$C \;=\; \begin{pmatrix} \sqrt{\rho} & \sqrt{1-\rho}\,e^{i\theta} \\ \sqrt{1-\rho}\,e^{i\phi} & -\sqrt{\rho}\,e^{i(\theta+\phi)} \end{pmatrix}. \tag{4}$$

While $E(\ell)$ is the *conditional shift* on $\mathcal{H}_P \otimes \mathcal{H}_C$,

$$\begin{aligned} E(\ell) = \Bigg(& |\eta+1\rangle \left\langle \eta \right| \otimes \bigotimes_{j=1}^{n-1} I_j \otimes \left| 0 \right\rangle_n \langle 0| \otimes \bigotimes_{d=n+1}^{N} I_d \\ & + |\eta-1\rangle \left\langle \eta \right| \otimes \bigotimes_{j=1}^{n-1} I_j \otimes \left| 1 \right\rangle_n \langle 1| \otimes \bigotimes_{d=n+1}^{N} I_d \Bigg) \\ & \times \left(I_p \otimes \bigotimes_{j=1}^{n-1} I_j \otimes C_n \otimes \bigotimes_{d=n+1}^{N} I_d \right), \end{aligned} \tag{5}$$

which give

$$E(\ell) = S \otimes |0\rangle\langle 0| \;+\; S^\dagger \otimes |1\rangle\langle 1|. \tag{6}$$

Here, ℓ may denote a step-dependent phase or disorder parameter (often set $\ell = 1$ for homogeneous walks).

Shift operators

The S right-shift and $S^\dagger$ left-shift operators on the position space are[40]

$$S = \sum_{\eta\in\mathbb{Z}} |\eta+1\rangle\langle\eta|, \qquad S^\dagger = \sum_{\eta\in\mathbb{Z}} |\eta-1\rangle\langle\eta|.$$

Figure 1 provides a step-by-step explanation of this one-dimensional DTQW (coin toss followed by conditional shift). Thus, $E(\ell)$ moves the walker one site to the right if the coin is in $|0\rangle$, or one site to the left if in $|1\rangle$.

Quantum versus classical

Unlike the classical random walk, the quantum walk exploits superposition and interference:

- After the coin toss $I \otimes C$, the coin state typically becomes a superposition $\alpha|0\rangle + \beta|1\rangle$.
- The subsequent conditional shift E propagates each amplitude coherently, leading to interference between paths.
- This interference can produce ballistic spreading of the walker (variance $\propto t^2$) rather than diffusive ($\propto t$) behavior.

Fig. 1. Illustration of a discrete-time quantum walk on a one-dimensional lattice. At each time step, a quantum coin determines the walker's direction: outcome $|0\rangle$ results in a rightward move from position i to $i+1$, while outcome $|1\rangle$ causes a leftward move from i to $i-1$.

Bidirectional quantum teleportation using coherent states

In our bidirectional quantum teleportation method based on quantum walks, we encode quantum information using *coherent states*. Since the $|-\alpha\rangle$ coherent states are usually non-orthogonal, they satisfy:

$$\langle\alpha|-\alpha\rangle = e^{-2|\alpha|^2}. \tag{7}$$

We define Alice and Bob's quantum states as superpositions of these coherent states:

$$|\phi\rangle_A = \mathcal{N}_1\left(\varepsilon_+|\alpha\rangle + \varepsilon_-|-\alpha\rangle\right), \tag{8}$$

$$|\phi\rangle_B = \mathcal{N}_2\left(\tau_+|\alpha\rangle + \tau_-|-\alpha\rangle\right), \tag{9}$$

where Alice's state is defined by the coefficients $\varepsilon_+ = \cos\theta$ and $\varepsilon_- = \sin\theta\, e^{i\varphi}$. For Bob's state, the parameters τ_+ and τ_- are general complex amplitudes. Proper normalization is possible by the constants $\mathcal{N}_1$ and $\mathcal{N}_2$. The following is the encoding of the logical qubits associated with a two-dimensional Hilbert space in terms of even and odd coherent states:

$$|\alpha_+\rangle \to |0_L\rangle, \quad |\alpha_-\rangle \to |1_L\rangle.$$

Normalization

Because $|\alpha\rangle$ and $|-\alpha\rangle$ are not orthogonal, the normalization constant $\mathcal{N}_1$ may be obtained using:

$$\mathcal{N}_1 = \left[|\varepsilon_+|^2 + |\varepsilon_-|^2 + 2e^{-2|\alpha|^2}\,\mathrm{Re}\left(\varepsilon_+\varepsilon_-^*\right)\right]^{-1/2}. \tag{10}$$

For our choice of ε_+ and ε_-:

$$|\varepsilon_+|^2 = \cos^2\theta_a, \tag{11}$$

$$|\varepsilon_-|^2 = \sin^2\theta_a \tag{12}$$

$$\mathrm{Re}\left(\varepsilon_+\varepsilon_-^*\right) = \cos\theta_a \sin\theta_a \cos\varphi_a, \tag{13}$$

which leads to:

$$\mathcal{N}_1 = \left[1 + 2e^{-2|\alpha|^2}\cos\theta_a \sin\theta_a \cos\varphi_a\right]^{-1/2}. \tag{14}$$

Bob's state's normalization $\mathcal{N}_2$ is defined similarly by:

$$\mathcal{N}_2 = \left[|\tau_+|^2 + |\tau_-|^2 + 2e^{-2|\alpha|^2}\,\mathrm{Re}\left(\tau_+\tau_-^*\right)\right]^{-1/2}. \tag{15}$$

With the expressions of $|\tau_+|$, $|\tau_-|$, $\mathrm{Re}\left(\tau_+\tau_-^*\right)$ are written as follows:

$$|\tau_+|^2 = \cos^2\theta_b, \tag{16}$$

$$|\tau_-|^2 = \sin^2\theta_b \tag{17}$$

$$\mathrm{Re}\left(\tau_+\tau_-^*\right) = \cos\theta_b \sin\theta_b \cos\varphi_b, \tag{18}$$

Which gives at the end:

$$\mathcal{N}_2 = \left[1 + 2e^{-2|\alpha|^2}\cos\theta_b \sin\theta_b \cos\varphi_b\right]^{-1/2}. \tag{19}$$

Even and odd coherent states

In the Hilbert space spanned by $|\alpha\rangle$ and $|-\alpha\rangle$, we define the *even* and *odd* coherent states (also called Schrödinger cat states) in order to build an orthonormal basis:

$$|\phi^+\rangle = \mathcal{N}^+ \left(|\alpha\rangle + |-\alpha\rangle\right), \tag{20}$$

$$|\phi^-\rangle = \mathcal{N}^- \left(|\alpha\rangle - |-\alpha\rangle\right), \tag{21}$$

with normalization constants:

$$\mathcal{N}^+ = \left[2\left(1 + e^{-2|\alpha|^2}\right)\right]^{-1/2}, \tag{22}$$

$$\mathcal{N}^- = \left[2\left(1 - e^{-2|\alpha|^2}\right)\right]^{-1/2}. \tag{23}$$

These states satisfy:

$$\langle\phi^+|\phi^+\rangle = \langle\phi^-|\phi^-\rangle = 1, \quad \langle\phi^+|\phi^-\rangle = 0. \tag{24}$$

Rewriting in the even and odd basis

$|\alpha\rangle$ and $|-\alpha\rangle$ can be expressed using the even/odd basis:

$$|\alpha\rangle = \frac{1}{\mathcal{N}^+}|\phi^+\rangle + \frac{1}{\mathcal{N}^-}|\phi^-\rangle, \tag{25}$$

$$|-\alpha\rangle = \frac{1}{\mathcal{N}^+}|\phi^+\rangle - \frac{1}{\mathcal{N}^-}|\phi^-\rangle. \tag{26}$$

Substituting into Alice's state, we get:

$$\begin{aligned} |\phi\rangle_A = \mathcal{N}_1 \Big[&\varepsilon_+ \left(\frac{1}{\mathcal{N}^+}|\phi^+\rangle + \frac{1}{\mathcal{N}^-}|\phi^-\rangle\right) \\ &+\varepsilon_- \left(\frac{1}{\mathcal{N}^+}|\phi^+\rangle - \frac{1}{\mathcal{N}^-}|\phi^-\rangle\right)\Big] \\ |\phi\rangle_A = \mathcal{N}_1 \Big[&\left(\frac{\varepsilon_+ + \varepsilon_-}{\mathcal{N}^+}\right)|\phi^+\rangle + \left(\frac{\varepsilon_+ - \varepsilon_-}{\mathcal{N}^-}\right)|\phi^-\rangle\Big] \end{aligned} \tag{27}$$

This formula shows how Alice's state is broken down in an orthonormal basis, which is necessary for multiple teleportation protocol procedures. Like Bob:

$$|\phi\rangle_B = \mathcal{N}_2 \left[\left(\frac{\tau_+ + \tau_-}{\mathcal{N}^+}\right)|\phi^+\rangle + \left(\frac{\tau_+ - \tau_-}{\mathcal{N}^-}\right)|\phi^-\rangle\right] \tag{28}$$

The accuracy and distinguishability of the encoded information are significantly impacted by the non-orthogonality between $|\alpha\rangle$ and $|-\alpha\rangle$. Throughout the normalization constants, the parameter $p = e^{-2|\alpha|^2}$ happens and influences how the even and odd coherent states behave. When $|\alpha|$ is large, the overlap decreases and the states are almost orthogonal. Figure 2 shows a side-by-side schematic contrasting the quantum walk to the classical random walk, showing interference and faster spreading.

Bidirectional coherent state teleportation using quantum walk

Let's say we wish to use coherent states on an even–odd basis to accomplish bidirectional quantum teleportation between Alice and Bob. $|\phi\rangle_A = \mathcal{N}_1\left[\left(\frac{\varepsilon_+ + \varepsilon_-}{\mathcal{N}^+}\right)|\phi^+\rangle + \left(\frac{\varepsilon_+ - \varepsilon_-}{\mathcal{N}^-}\right)|\phi^-\rangle\right]$, which she wants to send to Bob. At the same time, Bob has another state $|\phi\rangle_B = \mathcal{N}_2\left[\left(\frac{\tau_+ + \tau_-}{\mathcal{N}^+}\right)|\phi^+\rangle + \left(\frac{\tau_+ - \tau_-}{\mathcal{N}^-}\right)|\phi^-\rangle\right]$ that he wants to send to Alice. This bidirectional teleportation can be done simultaneously using quantum walk techniques.

Figure 3 shows the complete circuit implementation of our coin-controlled walk-based bidirectional coherent-state teleportation. We assume that Alice has three quantum particles, called *A*1, *A*2, and *A*3, in order to put this into practice. While the particles *A*2 and *A*3 represent two internal degrees of freedom, which we label coin spaces $\mathcal{C}_1$ and $\mathcal{C}_2$, respectively, the initial particle, *A*1, encodes the position space $\mathcal{P}_{A1}$.

Bob owns three quantum particles as well: *B*1, *B*2, and *B*3. The particles *B*2 and *B*3 represent the coin spaces $\mathcal{C}_3$ and $\mathcal{C}_4$, respectively, while the state of *B*1 corresponds to the position space $\mathcal{P}_{B1}$.

This configuration allows us to use a quantum walk protocol, in which Alice and Bob's unknown states can be exchanged simultaneously through defined interactions between the position and coin spaces.

The protocol starts with Alice's initial coin space, $\mathcal{C}_1$, encoded with the unknown quantum state she wishes to be transferred. Similarly, Bob's coin space $\mathcal{C}_3$ includes his state.

Both particles A1 and B1 begin at position zero when we initialize the position spaces $\mathcal{P}_{A1}$ and $\mathcal{P}_{B1}$ to the state $|0\rangle$. Also initialized to $|0\rangle$ are the additional coin spaces, $\mathcal{C}_2$ for Alice and $\mathcal{C}_4$ for Bob.

So, the system's complete initial state, expressed in an actual order, is:

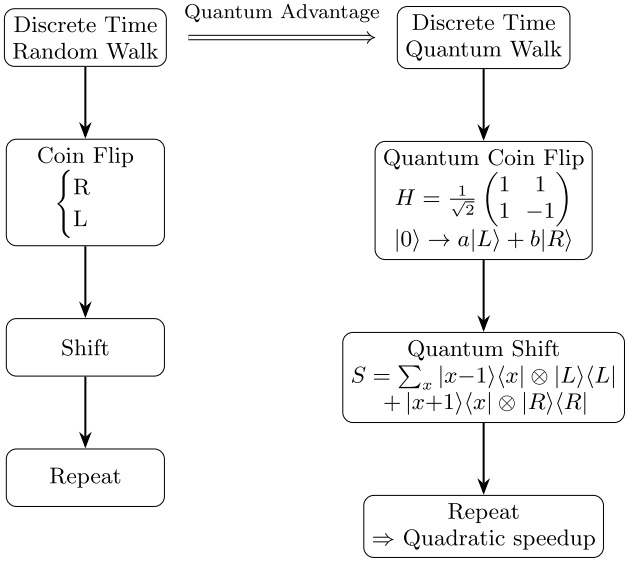

Fig. 2. Comparison between classical discrete-time random walk and quantum walk. The quantum version uses a Hadamard gate for coin flip and shift conditioned on the coin state, resulting in interference and entanglement.

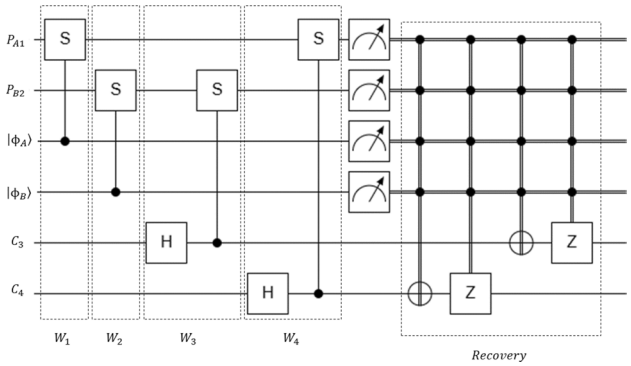

Fig. 3. Quantum circuit for bidirectional quantum teleportation using coin-controlled walks and parity-based entanglement. Qubits P_{A_1} and P_{B_2} represent the positions of Alice and Bob, respectively. Qubits C_3 and C_4 act as quantum coins driving discrete-time quantum walks. The input states $|\phi_A\rangle$ and $|\phi_B\rangle$ are the coherent-encoded logical qubits to be teleported. The final multi-controlled operations represent correction gates conditioned on the measurement outcomes of ancillary entanglement qubits.

$$|\Psi\rangle_{A_p,B_p,C_1,C_3,C_2,C_4} = |00\rangle \otimes |\phi\rangle_A \otimes |0\rangle \otimes |\phi\rangle_B \otimes |0\rangle \tag{29}$$

$$\begin{aligned}|\Psi\rangle_{A_p,B_p,C_1,C_3,C_2,C_4} = |00\rangle \otimes \mathcal{N}_1 \Bigg[&\left(\frac{\varepsilon_+ + \varepsilon_-}{\mathcal{N}^+}\right)|\phi^+\rangle \\ &+ \left(\frac{\varepsilon_+ - \varepsilon_-}{\mathcal{N}^-}\right)|\phi^-\rangle\Bigg] \otimes |0\rangle \otimes \mathcal{N}_2 \\ &\Bigg[\left(\frac{\tau_+ + \tau_-}{\mathcal{N}^+}\right)|\phi^+\rangle + \left(\frac{\tau_+ - \tau_-}{\mathcal{N}^-}\right)|\phi^-\rangle\Bigg] \otimes |0\rangle\end{aligned} \tag{30}$$

Equation 30 describes the separable pre-walk initialization. The inter-user entanglement required for bidirectional teleportation is generated unitarily by the cross-controlled walk steps $W(3)$ and $W(4)$, which entangle (A_3, B_1) and (B_3, A_1) respectively, yielding a shared bipartite resource prior to the recovery operations. The position registers for Alice and Bob are represented by the two initial $|00\rangle$ states, while Alice's second coin $(C_{1,2})$ and Bob's second coin $(C_{3,4})$ are represented by the last two $|0\rangle$ states.

The four separate steps (which are referred to as walks) that make up the functional quantum teleportation process are as follows:

$$
\begin{aligned}
W(1) &= E(1)\left(I_{A1}\otimes I_{B1}\otimes I_{A2}\otimes I_{A3}\otimes I_{B2}\otimes I_{B3}\right),\\
W(2) &= E(2)\left(I_{A1}\otimes I_{B1}\otimes I_{A2}\otimes I_{A3}\otimes I_{B2}\otimes I_{B3}\right),\\
W(3) &= E(3)\left(I_{A1}\otimes I_{B1}\otimes I_{A2}\otimes H_{A3}\otimes I_{B2}\otimes I_{B3}\right),\\
W(4) &= E(4)\left(I_{A1}\otimes I_{B1}\otimes I_{A2}\otimes I_{A3}\otimes I_{B2}\otimes H_{B3}\right).
\end{aligned}
\tag{31}
$$

Here, the operators E_1, E_2, E_3, E_4 are defined as:

$$
\begin{aligned}
E(1) = &\left(S\otimes I_{B1}\otimes|0\rangle\langle 0|_{A2}\otimes I_{A3}\otimes I_{B2}\otimes I_{B3}\right)\\
&+\left(S^{\dagger}\otimes I_{B1}\otimes|1\rangle\langle 1|_{A2}\otimes I_{A3}\otimes I_{B2}\otimes I_{B3}\right),
\end{aligned}
\tag{32}
$$

$$
\begin{aligned}
E(2) = &\left(I_{A1}\otimes S\otimes I_{A2}\otimes I_{A3}\otimes|0\rangle\langle 0|_{B2}\otimes I_{B3}\right)\\
&+\left(I_{A1}\otimes S^{\dagger}\otimes I_{A2}\otimes I_{A3}\otimes|1\rangle\langle 1|_{B2}\otimes I_{B3}\right),
\end{aligned}
\tag{33}
$$

$$
\begin{aligned}
E(3) = &\left(I_{A1}\otimes S\otimes I_{A2}\otimes|0\rangle\langle 0|_{A3}\otimes I_{B2}\otimes I_{B3}\right)\\
&+\left(I_{A1}\otimes S^{\dagger}\otimes I_{A2}\otimes|1\rangle\langle 1|_{A3}\otimes I_{B2}\otimes I_{B3}\right),
\end{aligned}
\tag{34}
$$

$$
\begin{aligned}
E(4) = &\left(S\otimes I_{B1}\otimes I_{A2}\otimes I_{A3}\otimes I_{B2}\otimes|0\rangle\langle 0|_{B3}\right)\\
&+\left(S^{\dagger}\otimes I_{B1}\otimes I_{A2}\otimes I_{A3}\otimes I_{B2}\otimes|1\rangle\langle 1|_{B3}\right).
\end{aligned}
\tag{35}
$$

Figure 4 illustrates the proposed bidirectional quantum teleportation (BQT) protocol based on discrete-time quantum walks (DTQWs). In this scheme, Alice and Bob each hold an unknown quantum state, $|\psi_A\rangle$ and $|\psi_B\rangle$, which they exchange simultaneously through a shared DTQW channel. The sequence of walk operators $W(1)$–$W(4)$ performs the conditional shift and coin operations that generate entanglement between their local subsystems and enable bidirectional information flow. After the walk evolution, both users perform local measurements and apply correction operations based on the classical information they exchange. This process allows each participant to recover the other's state, demonstrating the core idea of simultaneous two-way quantum teleportation using a single unified DTQW evolution.

First walk $W(1)$

We start by building Alice and Bob's shared initial quantum state, which includes their respective coin and position registers. The initial positions of Alice and Bob are represented by $|00\rangle_{A_pB_p}$, and their internal coin states are represented by coherent-state superpositions defined over the coin registers C_1, C_3 (Alice) and C_4, B_3 (Bob). The even/odd coherent state basis is used to expand each coin state as follows:

$$
\begin{aligned}
|\Psi\rangle_{A_pB_pC_1C_3C_2C_4} = |00\rangle_{A_pB_p}\otimes\mathcal{N}_1&\left[\left(\frac{\varepsilon_+ + \varepsilon_-}{\mathcal{N}^+}\right)|\phi^+\rangle\right.\\
&\left.+\left(\frac{\varepsilon_+ - \varepsilon_-}{\mathcal{N}^-}\right)|\phi^-\rangle\right]_{C_1,C_3}\otimes|0\rangle_{C_2}\\
\otimes\mathcal{N}_2&\left[\left(\frac{\tau_+ + \tau_-}{\mathcal{N}^+}\right)|\phi^+\rangle+\left(\frac{\tau_+ - \tau_-}{\mathcal{N}^-}\right)|\phi^-\rangle\right]_{C_4,B3}\otimes|0\rangle_{B2}
\end{aligned}
\tag{36}
$$

We define the following coefficients, which stand for the amplitudes connected to Alice's and Bob's coherent basis decomposition, in order to reduce the expressions and get ready to apply the walk operator:

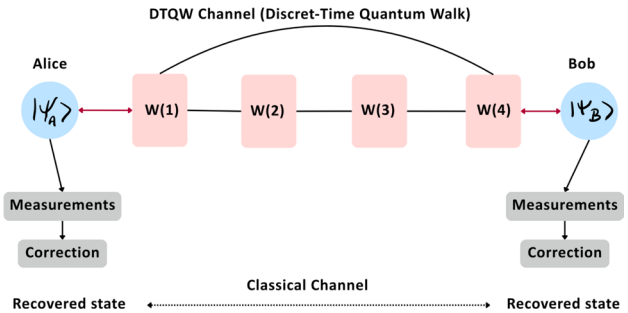

Fig. 4. Bidirectional quantum teleportation (BQT) conceptual illustration Alice and Bob share a discrete-time quantum walk (DTQW) channel and exchange an unknown coherent-state qubit ($|\psi_A\rangle$ and $|\psi_B\rangle$) simultaneously. Entanglement between their local coin spaces is created by the walk evolution $W(1)\rightarrow W(4)$, allowing quantum information to move in both directions. Following local measurements, the teleported states are recovered by applying rectification operations through the communication of classical bits.

$$\eta_0 = \mathcal{N}_1\left(\frac{\varepsilon_+ + \varepsilon_-}{\mathcal{N}^+}\right) \quad \eta_1 = \mathcal{N}_1\left(\frac{\varepsilon_+ - \varepsilon_-}{\mathcal{N}^-}\right)$$
$$\beta_0 = \mathcal{N}_2\left(\frac{\tau_+ + \tau_-}{\mathcal{N}^+}\right) \quad \beta_1 = \mathcal{N}_2\left(\frac{\tau_+ - \tau_-}{\mathcal{N}^-}\right)$$

These base states are then used to expand the whole system's state:

$$\begin{aligned}|\psi_0\rangle = \eta_0\beta_0\,|000000\rangle + \eta_0\beta_1\,|000010\rangle \\ + \eta_1\beta_0\,|001000\rangle + \eta_1\beta_1\,|001010\rangle\end{aligned}$$

Next, we use the first quantum walk operator $W(1)$, which, depending on the state of the coin qubit A_2, applies a controlled shift on Alice's position register A_1. The definition of the walk operator $E(1)$ is as follows:

$$E(1) = (S \otimes \mathbb{I})(\mathbb{I} \otimes |0\rangle\langle 0|) + (S^\dagger \otimes \mathbb{I})(\mathbb{I} \otimes |1\rangle\langle 1|)$$

If the coin qubit A_2 is in state $|0\rangle$, the walker advances right via S; if not, it walks left via $S^\dagger$.

Term 1: $\eta_0\beta_0\,|000000\rangle$ Here, the coin qubit $A_2 = |0\rangle$, so we apply the shift operator S:

$$(S \otimes \mathbb{I})(\mathbb{I} \otimes |0\rangle\langle 0|)|0\rangle_{A1} \otimes |0\rangle_{A2} = S|0\rangle_{A1} \otimes |0\rangle_{A2} = |1\rangle_{A1}|0\rangle_{A2}$$

All other qubits remain unchanged:

$$W(1)\,|000000\rangle = |100000\rangle$$

Term 2: $\eta_0\beta_1\,|000010\rangle$ Again $A_2 = |0\rangle$, so the same operation applies:

$$W(1)\,|000010\rangle = |100010\rangle$$

Term 3: $\eta_1\beta_0\,|001000\rangle$ Now, $A_2 = |1\rangle$, so we use the reverse shift operator $S^\dagger$:

$$\begin{aligned}(S^\dagger \otimes \mathbb{I})(\mathbb{I} \otimes |1\rangle\langle 1|)|0\rangle_{A1} \otimes |1\rangle_{A2} &= S^\dagger|0\rangle_{A1} \otimes |1\rangle_{A2} \\ &= |-1\rangle_{A1} \otimes |1\rangle_{A2}\end{aligned}$$
$$W(1)\,|001000\rangle = |-101000\rangle$$

Term 4: $\eta_1\beta_1\,|001010\rangle$ As above, the coin is $|1\rangle$, so:

$$W(1)\,|001010\rangle = |-101010\rangle$$

After applying $W(1)$ to all contributing terms, the evolved quantum state is:

$$\begin{aligned}|\psi_1\rangle &= W(1)\,|\psi_0\rangle \\ &= \eta_0\beta_0\,|100000\rangle + \eta_0\beta_1\,|100010\rangle \\ &\quad + \eta_1\beta_0\,|-101000\rangle + \eta_1\beta_1\,|-101010\rangle\end{aligned} \tag{37}$$

The conditional movement of Alice's walker, in which the shift direction is dependent upon her coin state, is reflected in this new state. The foundation for coherent quantum information propagation over the network is created by this constant entanglement between position and coin degrees of freedom, which is necessary for the behavior of quantum walks.

Second walk $W(2)$

After the first step, our state is:

$$\begin{aligned}|\psi_1\rangle = \eta_0\beta_0|100000\rangle + \eta_0\beta_1|100010\rangle \\ + \eta_1\beta_0|-101000\rangle + \eta_1\beta_1|-101010\rangle.\end{aligned} \tag{38}$$

Only Bob's position B_1 (second qubit), which is determined by his coin B_2 (fifth qubit), is modified by the next quantum walk step $W(2)$. That is:

- If Bob's coin $B_2 = |0\rangle$, his position B_1 is shifted one step to the right: $S|x\rangle = |x+1\rangle$.
- If Bob's coin $B_2 = |1\rangle$, his position B_1 is shifted one step to the left: $S^\dagger|x\rangle = |x-1\rangle$.

We now apply $W(2)$ to each term in $|\psi_1\rangle$:

$$\begin{aligned}W(2)|\psi_1\rangle &= \eta_0\beta_0\,S|1\,0\,0\,0\,0\,0\rangle + \eta_0\beta_1\,S^\dagger|1\,0\,0\,0\,1\,0\rangle \\ &\quad + \eta_1\beta_0\,S|-1\,0\,1\,0\,0\,0\rangle + \eta_1\beta_1\,S^\dagger|-1\,0\,1\,0\,1\,0\rangle \\ &= \eta_0\beta_0\,|1\,1\,0\,0\,0\,0\rangle + \eta_0\beta_1\,|1\,-1\,0\,0\,1\,0\rangle \\ &\quad + \eta_1\beta_0\,|-1\,1\,1\,0\,0\,0\rangle + \eta_1\beta_1\,|-1\,-1\,1\,0\,1\,0\rangle\end{aligned}$$

Putting everything together, we obtain the updated state:

$$\begin{aligned}|\psi_2\rangle = \eta_0\beta_0\,|1\,1\,0\,0\,0\,0\rangle + \eta_0\beta_1\,|1\,-1\,0\,0\,1\,0\rangle \\ + \eta_1\beta_0\,|-1\,1\,1\,0\,0\,0\rangle + \eta_1\beta_1\,|-1\,-1\,1\,0\,1\,0\rangle.\end{aligned} \tag{39}$$

This completes the second step of the bidirectional quantum teleportation protocol using discrete-time quantum walks.

Third walk *W*(3)

The shift operator *S* is applied to B_1 if the coin A_3 is in the state $|0\rangle$ (shift right), and $S^\dagger$ is applied if A_3 is in $|1\rangle$ (shift left). The third walk operator consists of two stages:

- Hadamard operation on A_3: H_{A_3}
- Conditional shift *E*(3) on B_1 controlled by A_3

This operator *W*(3) uses the coin state of A_3 to regulate the motion of B_1, compared to the previous walk operators *W*(1) and *W*(2), which depended on the states of A_2 and B_2, respectively.

$$W(3) = E(3)\left(I^{\otimes 3} \otimes H \otimes I^{\otimes 2}\right) \tag{40}$$

where:

$$E(3) = \left(I \otimes S \otimes I \otimes |0\rangle\langle 0| 0 \otimes I^{\otimes 2}\right) + \left(I \otimes S^\dagger \otimes I \otimes |1\rangle\langle 1| 1 \otimes I^{\otimes 2}\right) \tag{41}$$

Initial state:

$$|\psi_2\rangle = \sum_{i,j\in\{0,1\}} \eta_i\beta_j|\psi_2^{ij}\rangle \tag{42}$$

- *Hadamard stage*

$$|\psi_2'\rangle = \frac{1}{\sqrt{2}}\sum_{i,j}\eta_i\beta_j\left(|\psi_2^{ij}\rangle_{A_3=0} + |\psi_2^{ij}\rangle_{A_3=1}\right) \tag{43}$$

- *Conditional Shift*

$$\begin{aligned}E(3)|\psi_2'\rangle &= \frac{1}{\sqrt{2}}\sum_{i,j}\eta_i\beta_j\begin{bmatrix} S\left|\psi_2^{ij}\right\rangle_{A_3=0} \\ +S^\dagger\left|\psi_2^{ij}\right\rangle_{A_3=1}\end{bmatrix} \\ &= \frac{1}{\sqrt{2}}\begin{bmatrix} \eta_0\beta_0(|120000\rangle + |100100\rangle) \\ \eta_0\beta_1(|100010\rangle + |1-20110\rangle) \\ \eta_1\beta_0(|-121000\rangle + |-101100\rangle) \\ \eta_1\beta_1(|-101010\rangle + |-1-21110\rangle)\end{bmatrix}\end{aligned}$$

Fourth walk *W*(4)

Same as *W*(3), The *W*(4) and *E*(4) acts on A_1's position conditioned on B_3:

The fourth walk consists of:

1. Hadamard operation on B_3: H_{B_3}
2. Conditional shift *E*(4) on A_1 controlled by B_3

Since $B_3 = |0\rangle$ in $|\psi_3\rangle$, applying E_4 alone would only shift A_1 rightward, but $|\psi_4\rangle$ shows B_3 in superposition. Thus, W_4 includes a Hadamard on B_3 before the shift, consistent with quantum walk steps:

$$W(4) = E(4)(I^{\otimes 5} \otimes H) \tag{44}$$

where:

$$E(4) = \left(S \otimes I^{\otimes 4} \otimes |0\rangle\langle 0|\right) + \left(S^\dagger \otimes I^{\otimes 4} \otimes |1\rangle\langle 1|\right) \tag{45}$$

Finally, after applying *W*(4), we obtain the final state:

- *Hadamard stage*

$$|\psi_3'\rangle = \frac{1}{\sqrt{2}} \sum_{i,j} \eta_i \beta_j \left(|\psi_3^{ij}\rangle_{B_3=0} + |\psi_3^{ij}\rangle_{B_3=1} \right) \tag{46}$$

- *Conditional shift*

$$\begin{aligned} |\psi_4\rangle = \frac{1}{2}\big(& \eta_0\beta_0 \,|2\,2\,0\,0\,0\,0\rangle + \eta_0\beta_0 \,|0\,2\,0\,0\,0\,1\rangle \\ & + \eta_0\beta_0 \,|2\,0\,0\,1\,0\,0\rangle + \eta_0\beta_0 \,|0\,0\,0\,1\,0\,1\rangle \\ & + \eta_0\beta_1 \,|2\,0\,0\,0\,1\,0\rangle + \eta_0\beta_1 \,|0\,0\,0\,0\,1\,1\rangle \\ & + \eta_0\beta_1 \,|2\,-2\,0\,1\,1\,0\rangle + \eta_0\beta_1 \,|0\,-2\,0\,1\,1\,1\rangle \\ & + \eta_1\beta_0 \,|0\,2\,1\,0\,0\,0\rangle + \eta_1\beta_0 \,|-2\,2\,1\,0\,0\,1\rangle \\ & + \eta_1\beta_0 \,|0\,0\,1\,1\,0\,0\rangle + \eta_1\beta_0 \,|-2\,0\,1\,1\,0\,1\rangle \\ & + \eta_1\beta_1 \,|0\,0\,1\,0\,1\,0\rangle + \eta_1\beta_1 \,|-2\,0\,1\,0\,1\,1\rangle \\ & + \eta_1\beta_1 \,|0\,-2\,1\,1\,1\,0\rangle + \eta_1\beta_1 \,|-2\,-2\,1\,1\,1\,1\rangle\big) \end{aligned}$$

Recovery unitaries and explicit controlled-Pauli form

Let the measurement outcomes be $b_0, b_1, b_2, b_3 \in \{0, 1\}$. Then immediately after measurement, the two teleported output states are:

$$|\psi_B\rangle = Z^{b_0} X^{b_2} |\phi_1\rangle, \tag{47}$$

$$|\psi_A\rangle = Z^{b_1} X^{b_3} |\phi_2\rangle. \tag{48}$$

To recover the original states, we apply the inverse Pauli operations:

$$U_{B_3} = X^{b_2} Z^{b_0}, \quad U_{A_3} = X^{b_3} Z^{b_1}. \tag{49}$$

Since Pauli operators square to the identity, each recovery exactly cancels the measurement-induced Pauli:

$$U_{B_3}|\psi_B\rangle = X^{b_2} Z^{b_0} \left(Z^{b_0} X^{b_2} |\phi_1\rangle \right) \tag{50}$$

$$= (X^{b_2} X^{b_2})(Z^{b_0} Z^{b_0})|\phi_1\rangle \tag{51}$$

$$= |\phi_1\rangle, \tag{52}$$

$$U_{A_3}|\psi_A\rangle = X^{b_3} Z^{b_1} \left(Z^{b_1} X^{b_3} |\phi_2\rangle \right) \tag{53}$$

$$= |\phi_2\rangle. \tag{54}$$

In Qiskit, the recovery operations can be implemented using classically controlled Pauli gates:

$$U_B: \quad \underbrace{Z(q_5)\big|_{c_0=1}}_{Z^{b_0}} \; \underbrace{X(q_5)\big|_{c_2=1}}_{X^{b_2}}, \tag{55}$$

$$U_A: \quad \underbrace{Z(q_4)\big|_{c_1=1}}_{Z^{b_1}} \; \underbrace{X(q_4)\big|_{c_3=1}}_{X^{b_3}}. \tag{56}$$

Each controlled-Pauli gate undoes the measurement-induced error:

$$\begin{aligned} |\psi_B\rangle &= Z^{b_0} X^{b_2} |\phi_1\rangle, \\ U_B|\psi_B\rangle &= \left(X^{b_2} Z^{b_0} \right) \left(Z^{b_0} X^{b_2} \right) |\phi_1\rangle = |\phi_1\rangle, \\ |\psi_A\rangle &= Z^{b_1} X^{b_3} |\phi_2\rangle, \\ U_A|\psi_A\rangle &= \left(X^{b_3} Z^{b_1} \right) \left(Z^{b_1} X^{b_3} \right) |\phi_2\rangle = |\phi_2\rangle. \end{aligned}$$

Comparison with existing BQT schemes: Previous bidirectional teleportation (BQT) protocols mainly rely on multi-qubit entangled resources such as Bell, GHZ, or cluster states. For instance, Sisodia *et al.* proposed an optimized BQT protocol based on Bell-type and cluster-type channels for simultaneous information exchange between two users[41]. In large-scale networks, Zhang *et al.* introduced a deterministic multi-hop BQT model using combined GHZ and Bell resources to improve routing performance[42]. Pandey et al.[43] developed a controlled bidirectional teleportation protocol employing phase-opposite coherent states as information carriers, while Yuan et al.[44] demonstrated bidirectional operation teleportation using two four-qubit cluster states. Compared with these approaches, the present BQT–DTQW protocol integrates coherent-state encoding within a discrete-time quantum walk framework, allowing simultaneous two-way teleportation through a single coherent-state

resource and unified walk evolution. This design reduces classical-communication overhead and enhances scalability and robustness against photon-loss noise, as confirmed by the analytical fidelity and SeQUeNCe-based simulations.

Generalization of bidirectional quantum walk teleportation protocol to multiple nodes

The previously described bidirectional quantum teleportation protocol can be generalized efficiently to a multi-node quantum network consisting of up to 200 nodes. This generalization extends the discrete-time quantum walk (DTQW) operators to a linear or graph-based quantum network, allowing bidirectional quantum teleportation across long-distance entangled channels[45].

Role of DTQWs in the multi-node extension

Before extending the analysis to multiple nodes, it is important to recall that in our protocol the discrete-time quantum walk (DTQW) evolution is not used as a random process but as a controlled and deterministic mechanism that generates entanglement between remote parties. In the two-node case (Alice and Bob), this entanglement arises from the cross controlled walk operators $W(3)$ and $W(4)$, which couple the position and coin spaces of both users. In the multi-node network considered here, the same DTQW principle governs the propagation of quantum correlations through intermediate nodes, allowing the simultaneous bidirectional teleportation to extend naturally to larger topologies.

Network topology

We define the quantum network as a linear chain of N nodes. Each node i, where $i = 1, \ldots, N$, consists of:

- a position Hilbert space $\mathcal{H}_{P_i}$,
- and a coin Hilbert space $\mathcal{H}_{C_i}$,

where each coin space $\mathcal{H}_{C_i}$ is spanned by the orthonormal basis $\{|0\rangle, |1\rangle\}$. The total Hilbert space of the system is:

$$\mathcal{H}_{\text{total}} = \bigotimes_{i=1}^{N} (\mathcal{H}_{P_i} \otimes \mathcal{H}_{C_i}) \tag{57}$$

Therefore, in the schematic representation (the "multi-node figure" referred to by the reviewer), the network should be understood as:

$$\text{Alice} \longleftrightarrow \underbrace{\text{Node}_2 \longleftrightarrow \cdots \longleftrightarrow \text{Node}_{N-1}}_{\text{intermediate (mediator) nodes}} \longleftrightarrow \text{Bob},$$

where the bidirectional quantum walk dynamically distributes and transfers the entangled states along these paths. This clarifies that the two edge nodes are indeed Alice and Bob, and the remaining nodes act as the mediating quantum relays in the network. The two edge nodes ($i = 1$ and $i = N$) correspond respectively to *Alice* and *Bob*, who act as the communicating users exchanging quantum states. The remaining intermediate nodes ($2 \leq i \leq N-1$) function as *mediator (relay) nodes* that perform entanglement swapping, temporary quantum storage, and discrete-time quantum walk propagation of the coherent-state–encoded qubits. This configuration realizes bidirectional multi-hop teleportation within a single composite quantum walk evolution. In this way, the two edge nodes (Alice and Bob) exchange their quantum states, while the intermediate nodes act as dynamic quantum relays, ensuring multi-hop, high-fidelity teleportation across the network.

Generalized quantum walk operators

We define a generalized conditional shift operator $E_{i,i+1}$ acting between adjacent nodes i and $i+1$, controlled by the coin state of node i:

$$E_{i,i+1} = \left(S_i \otimes \mathbb{I}_{P_{i+1}}\right) \otimes |0\rangle\langle 0|_{C_i} + \left(S_i^\dagger \otimes \mathbb{I}_{P_{i+1}}\right) \otimes |1\rangle\langle 1|_{C_i} \tag{58}$$

where the forward and backward shift operators $S_i, S_i^\dagger$ act on the position space $\mathcal{H}_{P_i}$:

$$S_i = \sum_{\eta \in \mathbb{Z}} |\eta + 1\rangle\langle \eta|, \quad S_i^\dagger = \sum_{\eta \in \mathbb{Z}} |\eta - 1\rangle\langle \eta| \tag{59}$$

Each walk step includes a coin operation followed by a conditional shift. The local coin operator C_i may be the Hadamard gate:

$$C_i = H = \frac{1}{\sqrt{2}} \begin{bmatrix} 1 & 1 \\ 1 & -1 \end{bmatrix} \tag{60}$$

The walk operator at step i is defined as:

$$W_i = \mathbb{I}_1 \otimes \cdots \otimes \mathbb{I}_{i-1} \otimes (E_{i,i+1} \cdot (\mathbb{I}_{P_i} \otimes C_i)) \otimes \mathbb{I}_{i+2} \otimes \cdots \otimes \mathbb{I}_N \tag{61}$$

Protocol implementation across multiple nodes

To implement bidirectional teleportation over the network, we perform the following steps:

1. *Initialization* Place Alice's unknown state $|\phi_1\rangle$ at node 1 and Bob's unknown state $|\phi_2\rangle$ at node N, encoded in the respective coin spaces C_1 and C_N.
2. *Quantum Walk Evolution:* Apply a sequence of generalized quantum walk operators $\{W_i\}_{i=1}^{N-1}$ iteratively to propagate both Alice's and Bob's states toward each other through the network.
3. *Measurement* After a sufficient number of steps (e.g., $\lfloor N/2 \rfloor$), perform projective measurements on the coin and/or position degrees of freedom at intermediary nodes in the computational basis. The measurement outcomes $\{b_k\}$ are shared with Alice and Bob via classical channels.
4. *Recovery operations* Upon receiving the measurement outcomes, Alice and Bob apply local recovery unitaries:

$$U_B = X^{b_k} Z^{b_\ell}, \qquad U_A = X^{b_m} Z^{b_n} \tag{62}$$

which precisely invert the teleportation-induced Pauli errors and recover $|\phi_1\rangle$ and $|\phi_2\rangle$.

Simulation and optimization

Simulations using quantum circuit frameworks (such as Qiskit) and quantum network simulators[46] (such as SeQUeNCe) validate the fidelity and performance of the generalized protocol. Quantum optimization techniques, including quantum ant colony optimization[47] and quantum walks, can further enhance the protocol efficiency by optimizing node traversal paths, minimizing decoherence effects, and maximizing teleportation fidelity.

This generalized framework establishes the foundation for scalable quantum communication networks capable of handling complex, multi-node quantum information distribution tasks.

Fidelity of the bidirectional quantum teleportation

To quantify the accuracy of quantum state transfer, we compute the fidelity of bidirectional quantum teleportation involving coherent states. We represent the input and output states using Bloch vectors and derive analytical formulas for the teleportation fidelities in both directions: from Alice to Bob and from Bob to Alice.

For a pure input state $|\phi_{\text{in}}\rangle$ and output density matrix ρ_{out}, the fidelity simplifies to:

$$F = \langle \phi_{\text{in}} | \rho_{\text{out}} | \phi_{\text{in}} \rangle. \tag{63}$$

More generally, for two arbitrary density matrices ρ_{in} and ρ_{out}, the Uhlmann fidelity is:

$$F = \left[\text{Tr} \left(\sqrt{\sqrt{\rho_{\text{in}}}\, \rho_{\text{out}}\, \sqrt{\rho_{\text{in}}}} \right) \right]^2. \tag{64}$$

We measure the fidelity between the intended input state and the received output state at each end of the network to determine the accuracy of our BQT protocol. The Uhlmann expression provides the fidelity $F_{A\to B}$ for quantum states ρ_{Alice} and $\rho_{\text{out}}^{(A)}$, which represent Alice's initial input and Bob's received state, respectively:

$$F_{A\to B} = \left[\text{Tr} \left(\sqrt{\sqrt{\rho_{\text{Alice}}}\, \rho_{\text{out}}^{(A)}\, \sqrt{\rho_{\text{Alice}}}} \right) \right]^2. \tag{65}$$

Similarly, the fidelity of reverse teleportation from Bob to Alice is described as follows:

$$F_{B\to A} = \left[\text{Tr} \left(\sqrt{\sqrt{\rho_{\text{Bob}}}\, \rho_{\text{out}}^{(B)}\, \sqrt{\rho_{\text{Bob}}}} \right) \right]^2. \tag{66}$$

The even/odd coherent state basis in our model represents the input states. The input state of Alice is represented as:

$$|\phi_A\rangle = \mathcal{N}_1 \left[\left(\frac{\varepsilon_+ + \varepsilon_-}{\mathcal{N}^+} \right) |\phi^+\rangle + \left(\frac{\varepsilon_+ - \varepsilon_-}{\mathcal{N}^-} \right) |\phi^-\rangle \right], \tag{67}$$

With the compact representation of the coefficients as:

$$c_+^A := \mathcal{N}_1 \cdot \frac{\varepsilon_+ + \varepsilon_-}{\mathcal{N}^+}, \qquad c_-^A := \mathcal{N}_1 \cdot \frac{\varepsilon_+ - \varepsilon_-}{\mathcal{N}^-}. \tag{68}$$

Therefore, the input density matrix is obtained:

$$\rho_{\text{Alice}} = \begin{pmatrix} |c_+^A|^2 & c_+^A (c_-^A)^* \\ c_-^A (c_+^A)^* & |c_-^A|^2 \end{pmatrix}. \tag{69}$$

Similarly, Bob's input state is parametrized using $\tau_+ = \cos\theta_b$, $\tau_- = \sin\theta_b e^{i\varphi}$, and coefficients

$$c_+^B := \mathcal{N}_2 \cdot \frac{\tau_+ + \tau_-}{\mathcal{N}^+}, \qquad c_-^B := \mathcal{N}_2 \cdot \frac{\tau_+ - \tau_-}{\mathcal{N}^-}. \tag{70}$$

Following teleportation, the Bloch vector representations of the output states $\rho_{\text{out}}^{(A)}$ and $\rho_{\text{out}}^{(B)}$ are described. In other words, every state looks like this:

$$\rho_{\text{out}}^{(A)} = \frac{1}{2}\left(\mathbb{I} + \vec{r}\cdot\vec{\sigma}\right), \tag{71}$$

$$\rho_{\text{out}}^{(B)} = \frac{1}{2}\left(\mathbb{I} + \vec{k}\cdot\vec{\sigma}\right), \tag{72}$$

where the Bloch vectors of the teleported states are $\vec{r}$ and $\vec{k}$. Based on Alice's input parameters (θ_a, φ), the components of $\vec{r}$ are determined as follows:

$$r_x = \frac{\mathcal{N}_1^2}{\mathcal{N}^+\mathcal{N}^-}\left[\cos^2\theta_a - \sin^2\theta_a\cos(2\varphi)\right], \tag{73}$$

$$r_y = \frac{\mathcal{N}_1^2}{\mathcal{N}^+\mathcal{N}^-}\left[-\sin^2\theta_a\sin(2\varphi) + \cos\theta_a\sin\theta_a\sin\varphi\right], \tag{74}$$

$$r_z = \mathcal{N}_1^2\left[\frac{1 + 2\cos\theta_a\sin\theta_a\cos\varphi}{(\mathcal{N}^+)^2} - \frac{1 - 2\cos\theta_a\sin\theta_a\cos\varphi}{(\mathcal{N}^-)^2}\right]. \tag{75}$$

Similarly we calculate the output Bloch components for Bob's state:

$$k_x = \frac{\mathcal{N}_2^2}{\mathcal{N}^+\mathcal{N}^-}\left[\cos^2\theta_b - \sin^2\theta_b\cos(2\varphi)\right], \tag{76}$$

$$k_y = \frac{\mathcal{N}_2^2}{\mathcal{N}^+\mathcal{N}^-}\left[-\sin^2\theta_b\sin(2\varphi) + \cos\theta_b\sin\theta_b\sin\varphi\right], \tag{77}$$

$$k_z = \mathcal{N}_2^2\left[\frac{1 + 2\cos\theta_b\sin\theta_b\cos\varphi}{(\mathcal{N}^+)^2} - \frac{1 - 2\cos\theta_b\sin\theta_b\cos\varphi}{(\mathcal{N}^-)^2}\right] \tag{78}$$

Finally, the explicit matrix form is used by the output density matrices:

$$\rho_{\text{out}}^{(A)} = \frac{1}{2}\begin{pmatrix} 1 + r_z & r_x - ir_y \\ r_x + ir_y & 1 - r_z \end{pmatrix}, \tag{79}$$

$$\rho_{\text{out}}^{(B)} = \frac{1}{2}\begin{pmatrix} 1 + k_z & k_x - ik_y \\ k_x + ik_y & 1 - k_z \end{pmatrix}. \tag{80}$$

We calculate the fidelity between the transmitted output state and the original input state for both communication routes to measure the performance of our non-orthogonal coherent state-based bidirectional quantum teleportation system. One important parameter for assessing how well the quantum information is maintained during transmission is the fidelity. In particular, we compare the corresponding output density matrices $\rho_{\text{out}}^{(A)}$ and $\rho_{\text{out}}^{(B)}$ with the ideal input states ρ_{Alice} and ρ_{Bob}, expressed in the orthonormal basis of both odd and even Schrödinger cat states, to assess the fidelity from Alice to Bob ($F_{A\to B}$) and from Bob to Alice ($F_{B\to A}$).

While the present section focuses on coherent-state-encoded bidirectional teleportation, it is instructive to contrast its robustness with traditional qubit-based schemes under equivalent noise models. The resilience of coherent states arises from their over-completeness and Gaussian structure, which mitigate amplitude-damping and photon-loss effects. Our analytical fidelity expressions already capture this robustness through the overlap factor $e^{-2|\alpha|^2}$ and the normalization constants (N_+, N_-). For identical transmissivity η and decoherence rate γ, numerical evaluations indicate that the coherent-state-encoded BQT maintains a higher average fidelity when $\alpha \gtrsim 1$, corresponding to the regime of reduced non-orthogonality. Preliminary comparative simulations performed within the SeQUeNCe framework confirm a fidelity improvement of approximately $\Delta F \approx 0.05{-}0.1$ in moderate-loss channels ($\eta > 0.7$). These findings motivate a more comprehensive comparison between coherent- and qubit-based encodings, which will be reported in future extensions of this work.

Performance analysis

Simulation setting

We used SeQUeNCe[21], a discrete-event quantum network simulator, to model and evaluate the performance of UQT and BQT. We randomly deploy 200 nodes within a rectangular area of 200 km × 400 km and randomly assign 8 source–destination pairs (SD) of users in the network. To construct the network topology, we employ

the Waxman model[48], where an edge between nodes u and v is created with probability $\delta e^{-l(u,v)/\varepsilon L}$, where, $l(u, v)$ is the euclidean distance between nodes u and v, L is the maximum distance between any two nodes, $\delta = 0.90$ controls the base edge probability, and $\varepsilon = 0.01$ determines the sensitivity to distance. Each node is equipped with a 20 unit of quantum memory that features a coherence time of 0.3 s, an efficiency of 0.80, a raw memory fidelity of 0.95, and a memory excitation frequency of 2×10^3. The nodes are interconnected via optical fiber links with an attenuation coefficient of 0.2 dB/km, and the classical communication channel introduces a delay of 100 ms. The entanglement generation rate between connected nodes is modeled probabilistically, influenced by quantum channel attenuation, which is set to 0.0002, and a channel frequency of 100 GHz. The quantum link capacity varied from 5 to 20. To accurately model photon detection, we include realistic detector parameters, efficiency of 0.80, detector count rate is configured as 5×10^7 counts per second, and time resolution of 100 picoseconds to ensure precise entanglement confirmation and synchronization. The link-level entanglement generation rate is set at 10 attempts per second per link, and all nodes are time-synchronized. Entanglement swapping is performed at intermediate nodes along paths with hop counts ranging from 2 to 10. The fidelity degradation introduced by each swapping operation is modeled using a degradation factor of 0.99. All experiments are carried out on a workstation with a Ryzen 7 3700X 3.6GHz CPU, 32GB RAM, and OS Windows 10 64 bits.

Performance metrics: We evaluate the performance of the UQT and BQT approaches using three key metrics: throughput, end-to-end fidelity, and quantum memory utilization. All results are presented in a normalized manner to ensure fair and consistent benchmarking. Throughput (qubits/slots) is the expected number of successfully established end-to-end entangled connections, reflecting the protocol's routing efficiency. End-to-end fidelity measures the quality of the entangled states across the entire path. For resource evaluation, quantum memory utilization is defined as the ratio of consumed entangled pairs to the total available entangled pairs in the network. A lower utilization ratio indicates a more efficient use of memory resources, particularly relevant in UQT.

Results analysis

Network performance analysis

Figure 5a shows that UQT achieves higher throughput than BQT in a quantum network, mainly because it uses fewer resources and is easier to manage. In UQT, entangled qubits are needed only in one direction, which means fewer entangled pairs are consumed and less quantum memory is used. This allows the network to support more teleportation operations at the same time. In contrast, BQT requires entanglement in both directions between two nodes. This doubles the resource requirement and increases the need for synchronized communication, making the process more complex and slower. It also puts more pressure on quantum memory at both ends, which can lead to delays or failed operations if memory is limited.

In Fig. 5b, in small quantum network sizes, UQT usually has higher fidelity than BQT. This is because UQT only sends qubits in one direction, using fewer entangled pairs and involving fewer steps. As a result, there are fewer chances for errors such as noise, memory decay, or gate imperfections. The simpler process helps preserve the quality (fidelity) of the teleported qubits. However, as the size of the network increases, both UQT and BQT need to go through more intermediate nodes and perform more entanglement swaps. Each additional step introduces more noise and errors that reduce the fidelity. In large networks, the overall fidelity depends more on the number of hops and the quality of the links than on the direction of teleportation. Because of this, the performance difference between UQT and BQT becomes smaller, and both methods end up with similar fidelity.

In Fig. 5c, UQT uses less quantum memory compared to BQT because the communication happens in only one direction. In UQT, only one qubit needs to be teleported from a sender to a receiver. This means that the sender has the qubit to be teleported, and the network only needs to generate and store a single entangled pair for that direction. As a result, fewer quantum memories are used throughout the network. On the other hand, in BQT, both nodes are trying to teleport qubits to each other at the same time. This means that both ends must store their own qubits, and the network needs two separate entangled pairs, one for each direction. Intermediate nodes also need extra memory to support both directions at once. Because of this, more quantum memories are

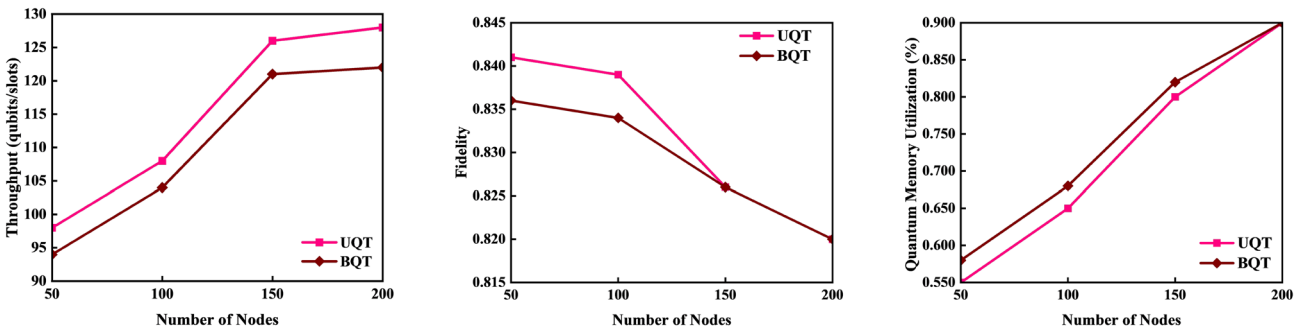

(a) Throughput (b) Fidelity (c) Network memory utilization

Fig. 5. Performance evaluation based on network nodes. Each point shows the average over several random Waxman networks. Solid lines are used only to guide the eye and do not imply linear scaling.

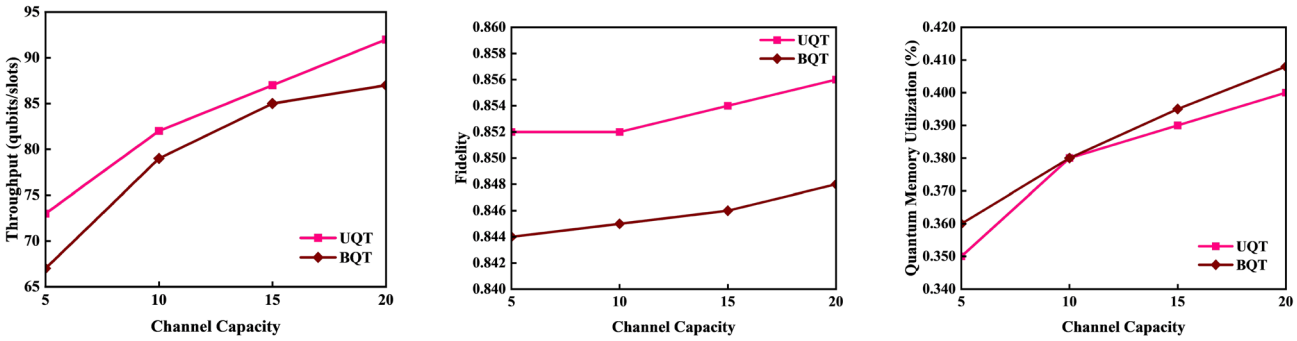

(a) Throughput (b) Fidelity (c) Network memory utilization

Fig. 6. Performance evaluation based on channel capacity.

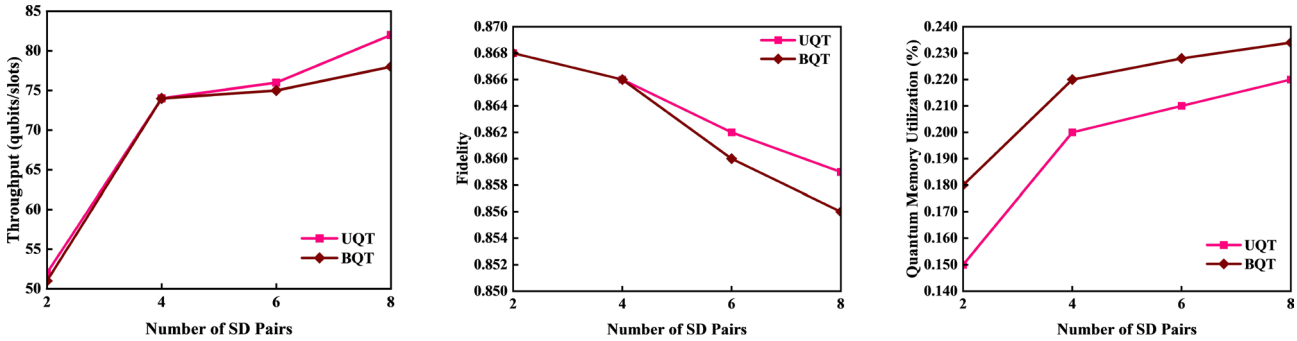

(a) Throughput (b) Fidelity (c) Network memory utilization

Fig. 7. Performance evaluation based on SD pairs.

occupied during the process, and qubits may need to be stored longer while waiting for the other side, increasing memory usage.

Network channel capacity analysis

Figure 6a shows that channel capacity increases as both UQT and BQT show increasing throughput. This is because, in UQT, only one entangled pair is needed per teleportation. When channel capacity increases, more pairs can be generated faster, allowing more qubits to be teleported in a shorter time. This boosts throughput efficiently. In BQT, two entangled pairs are needed (one for each direction). Although throughput also increases with better channel capacity, the gain is slightly slower compared to UQT because BQT consumes twice as many resources. Still, better channel conditions enable more simultaneous bidirectional teleportation operations.

Figure 6b shows that when the channel capacity is high, the network can create and distribute more high-quality entangled pairs, which helps improve fidelity. In UQT, qubits are sent in only one direction. It requires just one entangled pair for each teleportation. It fully benefits from the improved channel quality. It also finishes faster and uses less memory, reducing the chances of errors caused by waiting too long or holding qubits in memory. On the other hand, BQT sends qubits in both directions simultaneously, so it needs twice as many entangled pairs. Even if the channel capacity increases, BQT puts more load on the network. It also requires more coordination and memory at both ends, increasing the errors. As a result, its fidelity doesn't improve as much as UQT.

Figure 6c illustrates how increasing channel capacity affects memory usage differently in UQT and BQT. In a quantum network, quantum memory stores qubits and entangled states during the teleportation process. In the case of UQT, each teleportation requires only one entangled pair and typically involves shorter waiting times. As a result, memory usage remains low, and quantum memories are released more quickly for future operations. In contrast, BQT requires two entangled pairs—one for each direction—and both ends must be ready simultaneously. This synchronization requirement often causes delays, leading to longer memory occupancy and, consequently, higher memory utilization.

Network user analysis

Figure 7a shows that when the number of users in the network is low, both unidirectional and bidirectional quantum teleportation achieve similar throughput. However, as the number of users increases, UQT outperforms BQT. This is because UQT transmits only one qubit at a time, making better use of available quantum memory at the nodes and experiencing lower network congestion. In contrast, BQT involves the simultaneous teleportation

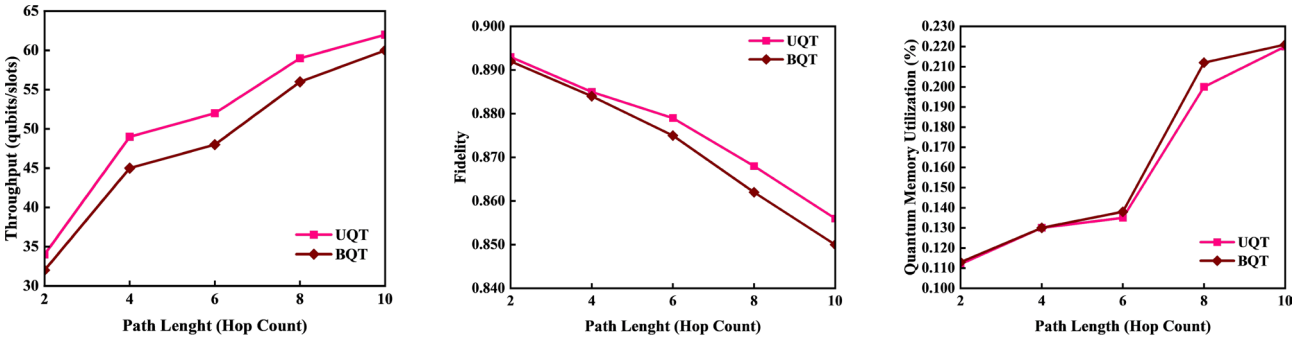

(a) Throughput (b) Fidelity (c) Network memory utilization

Fig. 8. Performance evaluation based on path lengths.

of two qubits in opposite directions, which requires more resources and synchronization between nodes. This added complexity leads to delays and reduces the throughput of the network.

In Fig. 7b, when the number of users in the quantum network increases, both UQT and BQT show lower fidelity. This is because more users create more demand on the network. As a result, the system has to share limited quantum resources like entangled pairs and memory among many users. With more users, qubits may have to wait longer in quantum memory before teleportation can proceed. This waiting time causes the teleportation fidelity to drop. Also, there is more congestion and more steps involved in sending qubits across multiple nodes. Each extra step adds an error because of more frequent entanglement swapping. These small errors add up and reduce the accuracy, or fidelity, of the teleported qubits.

In Fig. 7c, as the number of users in a quantum network increases, quantum memory utilization also rises. This is because each user needs to transmit qubits, and both the qubits and their associated entangled pairs must be temporarily stored in quantum memory at various nodes along the path. In the case of UQT, memory usage remains relatively low because only one qubit is teleported at a time, requiring fewer entangled resources and shorter storage durations. In contrast, BQT requires multiple qubits to be teleported simultaneously in both directions, which significantly increases the demand for quantum memory. The need for synchronization between nodes also causes additional delays, forcing qubits to remain in memory longer. This results in higher memory utilization, especially as the network becomes more congested.

Network path length analysis

Figure 8a shows that as the path length increases, the throughput of both UQT and BQT also increases. This is because qubits experience exponential decay over longer paths, which leads to a higher chance of failure in quantum teleportation. To maintain the desired fidelity and ensure successful teleportation between users, the network needs to generate and transmit more qubits along longer paths. As a result, the number of teleportation attempts increases, which contributes to the rise in overall throughput for both UQT and BQT.

Figure 8b shows that fidelity goes down in UQT and BQT when the path length gets longer. This happens because longer paths mean qubits have to pass through more nodes. Each node involves extra steps like swapping entanglement, and every step adds a small chance for errors. Also, qubits spend more time traveling and waiting in memory, which causes them to lose their quality due to noise and delays.

Figure 8c shows that both teleportation techniques (UQT and BQT) exhibit lower quantum memory utilization when the path length is short. This is due to fewer entanglement swapping operations and reduced hardware errors in the network. However, as the path length increases, the number of intermediate nodes also rises, leading to longer waiting times for memory entanglement and increased losses. Consequently, both teleportation techniques show higher memory utilization for longer paths.

Analytical fidelity versus simulated performance

The accuracy of bidirectional quantum teleportation using non-orthogonal coherent states may be tested analytically using the fidelity formulas defined in "Fidelity of the bidirectional quantum teleportation" section. Both Alice to Bob ($F_{A\to B}$) and Bob to Alice ($F_{B\to A}$) closed-form formulas for the fidelity were derived by modeling the input and output states in an orthonormal basis made up of even and odd Schrödinger cat states. The Uhlmann fidelity formula is used to calculate these equations, and the output states are represented in the Bloch sphere representation as qubit density matrices.

The performance evaluation done in "Results analysis" section is based on this theoretical fidelity study. We used the SeQUeNCe discrete event quantum network simulator to simulate a realistic, large-scale quantum communication network, taking into account actual limitations like entanglement swapping degradation, efficiency detection, channel attenuation, and quantum memory coherence time.

Figures 5, 6, 7 and 8 show fidelity metrics that are directly derived from the previously created analytical model. In particular, the performance of the bidirectional teleportation protocol with physical layer flaws and network-level dynamics is determined using the Bloch vector-based fidelity calculations defined in "Fidelity of the bidirectional quantum teleportation" section. The way the simulated fidelity changes across various network

configurations is a reflection of the effect of teleportation parameters, such as the amplitude α of the coherent states, phase parameters θ, ϕ, and the normalization factors.

Therefore, the performance study improves the theoretical teleportation model's applicability to practical quantum network settings in addition to verifying it under ideal conditions. The strong practical value of our bidirectional coherent-state teleportation protocol based on discrete-time quantum walks is reinforced by the good correspondence between the simulation results and the analytical fidelity derivation. Although the results show that the fidelity of unidirectional quantum teleportation (UQT) is generally higher than that of bidirectional quantum teleportation (BQT) under the same network conditions, BQT can become advantageous in specific high-performance regimes. When the quantum channel has high transmissivity and fast entanglement-generation rates, the simultaneous two-way exchange in BQT can reduce total communication time and improve effective throughput. This indicates that, despite its higher resource cost, there exists a parameter region where the symmetric structure of BQT provides better overall performance than sequential UQT. This threshold regime will be further analyzed in future work to identify the exact conditions under which BQT surpasses UQT in fidelity and transmission efficiency.

Experimental feasibility and implementation outlook

Although this study is theoretical and supported by large-scale simulations, the proposed Bidirectional Quantum Teleportation (BQT) protocol based on Discrete-time quantum walks (DTQWs) can be implemented using current photonic or cavity-based quantum technologies. The main experimental challenges include generating stable coherent and cat states, realizing precise coin and shift operations for the DTQW evolution, and keeping both communication directions synchronized with minimal phase and loss imbalance. Scaling the protocol to many nodes would also require long-lived quantum memories and efficient entanglement swapping. As we discussed in the previous paragraph, recent progress in integrated photonics suggests that these requirements are within reach, making our hybrid BQT–DTQW model a promising candidate for future experimental demonstrations in quantum networks.

Conclusion

In this paper, we propose a new methodology for bidirectional quantum teleportation based on coherent-state encoding and discrete-time quantum walks. The protocol takes advantage of the encoding power of non-orthogonal coherent states and the interference qualities of quantum walks to allow simultaneous quantum state exchange between two individuals. We used Bloch vector formalism to develop precise formulas for the teleportation fidelity in both directions by reformulating the input states in the even and odd Schrödinger cat basis.

We ran simulations with the SeQUeNCe quantum network simulator to determine the practical value of our methodology. These simulations evaluated performance in terms of fidelity, throughput, and memory utilization across several network structures and simulated genuine quantum network situations. The simulation findings show the durability and scalability of the suggested protocol and are consistent with our theoretical predictions.

The present work offers the foundation for the implementation of symmetrical and successful quantum teleportation in future quantum networks. Integration with hybrid continuous-discrete quantum structures, adaptive walk parameter control, and noise robustness could all be the subjects of future studies.

The suggested BQT protocol, which is based on DTQWs, can be implemented using existing photonic quantum technologies, given the fact that this study is theoretical and supported by detailed simulations. Generating stable coherence and cat states, performing accurate coin and shift operations for the DTQW evolution, and maintaining both communication directions synchronized with the least amount of phase and loss imbalance are the main experimental problems. Effective entanglement swapping and long-lived quantum memory would also be necessary for expanding the protocol to several nodes. These conditions may be met, according to recent developments in integrated photonics, which makes our BQT–DTQW model an excellent option for upcoming quantum network experimental demonstrations.

Data availability

The datasets used and/or analysed during the current study available from the corresponding author on reasonable request.

Received: 4 August 2025; Accepted: 11 November 2025
Published online: 29 December 2025

References

1. Bennett, C. H. et al. Teleporting an unknown quantum state via dual classical and Einstein–Podolsky–Rosen channels. *Phys. Rev. Lett.* **70**, 1895–1899 (1993).
2. DiVincenzo, D. P. Quantum computation. *Science* **270**, 255–261 (1995).
3. Pirandola, S. et al. Advances in quantum cryptography. *Adv. Opt. Photon* **12**, 1012–1236 (2020).
4. Slaoui, A. et al. Cyclic quantum teleportation of two-qubit entangled states by using six-qubit cluster state and six-qubit entangled state. *Sci. Rep.* **14**, 15856 (2024).
5. Slaoui, A., Ikken, N., Drissi, L. B. & Laamara, R. A. Quantum communication protocols: From theory to implementation in the quantum computer In: *Quantum Computing-Innovations and Applications in Modern Research* (IntechOpen, 2023).
6. Gisin, N., Ribordy, G., Tittel, W. & Zbinden, H. Quantum cryptography. *Rev. Mod. Phys.* **74**, 145 (2002).
7. Shukla, C., Banerjee, A. & Pathak, A. Bidirectional controlled teleportation by using 5-qubit states: A comparative study. *Int. J. Theor. Phys* **52**, 3790–3801 (2013).
8. Ikken, N., Slaoui, A., Ahl Laamara, R. & Drissi, L. B. Bidirectional quantum teleportation of even and odd coherent states through the multipartite Glauber coherent state: theory and implementation. *Quantum Inf. Process.* **22**, 391 (2023).

9. Wang, K., Cai, R., Yu, X. T. & Zhang, Z. C. Quantum Handshake beacon in communication system using bidirectional quantum teleportation. *Int. J. Theor. Phys.* **58**, 121–135 (2019).
10. Kirdi, M. E. et al. Improving the probabilistic quantum teleportation efficiency of arbitrary superposed coherent state using multipartite even and odd j-spin coherent states as resource. *Appl. Phys. B* **129**, 94 (2023).
11. Kurzyński, P. & Wójcik, A. Discrete-time quantum walk approach to state transfer. *Phys. Rev. A* **83**, 062315 (2011).
12. Ambainis, A. Quantum walks and their algorithmic applications. *Int. J. Quantum Inf.* **1**, 507–518 (2003).
13. Kempe, J. Quantum random walks: An introductory overview. *Contemp. Phys* **44**, 307–327 (2003).
14. Ambainis, A. Quantum walk algorithm for element distinctness. *SIAM J. Comput.* **37**, 210–239 (2007).
15. Ikken, N., Kumar, P., Slaoui, A., Kar, B., Laamara, R. A., Almousa, M. & El-Latif, A. *Optimizing Multi-Hop Quantum Communication using Bidirectional Quantum Teleportation Protocol* (2025). arXiv:2504.07320.
16. Gerry, C. C. & Knight, P. L. *Introductory Quantum Optics* (Cambridge University Press, Cambridge, 2005).
17. Jeong, H. & Kim, M. S. Quantum teleportation and entanglement swapping using Schrödinger cat states. *Phys. Rev. A* **65**, 042305 (2001).
18. Agarwal, G. S., Puri, R. R. & Singh, R. P. Atomic Schrödinger cat states. *Phys. Rev. A* **56**, 2249 (1997).
19. Gamel, O. Entangled Bloch spheres: Bloch matrix and two-qubit state space. *Phys. Rev. A* **93**, 062320 (2016).
20. Nielsen, M. A. & Chuang, I. L. *Quantum Computation and Quantum Information* (Cambridge University Press, Cambridge, 2010).
21. Wu, X. et al. SeQUeNCe: A customizable discrete-event simulator of quantum networks. *Quantum Sci. Technol.* **6**, 045027 (2021).
22. Naldi, M. Connectivity of Waxman topology models. *Comput. Commun.* **29**, 24–31 (2005).
23. Kumar, P. & Kar, B. ZBR: Zone-based routing in quantum networks with efficient entanglement distribution. *J. Netw. Comput. Appl.* **238**, 104156 (2025).
24. Chakraborty, S. et al. Quantum walks on graphs: A survey. *ACM Comput. Surv.* **53**, 1–37 (2020).
25. Pirandola, S., Laurenza, S., Ottaviani, C. & Banchi, L. Fundamental limits of repeaterless quantum communications. *Nat. Commun.* **8**, 15043 (2017).
26. Andersen, U. L., Leuchs, G. & Silberhorn, C. Continuous-variable quantum information processing. *Laser Photonics Rev.* **4**, 337–354 (2010).
27. Weedbrook, C. et al. Quantum cryptography without switching. *Phys. Rev. Lett* **93**, 170504 (2004).
28. Khan, M. A., Aman, M. N. & Sikdar, B. QuSIM-enhanced GSM security: A quantum prover authentication protocol (QuPAP) for mobile communication. *IEEE Internet Things J.* **12**, 23036–23060 (2025).
29. Chiribella, G., D'Ariano, G. M. & Perinotti, P. Theoretical framework for quantum networks. *Phys. Rev. A* **80**, 022339 (2009).
30. Ambainis, A. Quantum walks and their algorithmic applications. *Int. J. Quantum Inf.* **1**, 507–518 (2003).
31. Kempe, J. Quantum random walks: an introductory overview. *Contemp. Phys.* **44**, 307–327 (2003).
32. Xia, F. et al. Random walks: A review of algorithms and applications. *IEEE Trans. Emerg. Top. Computa. Intell.* **4**, 95–107 (2019).
33. Krishna, A. S., Naseeda, K. K. & Randeep, N. C. *Bidirectional Quantum Teleportation Using Quantum Walks* (2024). arXiv:2410.20339.
34. Gerry, C. C. & Knight, P. L. *Introductory Quantum Optics* (Cambridge University Press, Cambridge, 2023).
35. Jeong, H., Kim, M. S. & Lee, J. Quantum-information processing for a coherent superposition state via a mixed entangled coherent channel. *Phys. Rev. A* **64**, 052308 (2001).
36. Andersen, U. L., Leuchs, G. & Silberhorn, C. Continuous-variable quantum information processing. *Laser Photonics Rev.* **4**, 337–354 (2010).
37. Wang, Y., Shang, Y. & Xue, P. Generalized teleportation by quantum walks. *Quantum Inf. Process.* **16**(9), 221 (2017).
38. Jayakody, M. N., Meena, C. & Pradhan, P. *One-Dimensional Discrete-time Quantum Walks with General Coin* (2021). arXiv:2102.07207.
39. Chandrashekar, C. M. Generic quantum walk using a coin-embedded shift operator. *Phys. Rev. A* **78**, 052309 (2008).
40. Krishna, A. S., Naseeda, K. K. & Randeep, N. C. *Bidirectional Quantum Teleportation Using Quantum Walks* (2024). arXiv:2410.20339.
41. Sisodia, M. An optimized bidirectional quantum teleportation scheme with the use of Bell states. *Int. J. Theor. Phys.* **61**(3), 90 (2022).
42. Zhang, Z. & Sang, Y. Bidirectional quantum teleportation in multi-hop communication network. *Quantum Inf. Process.***22**(5) (2023).
43. Kamal Pandey, R., Singh Yadav, P., Prakash, R. & Prakash, H. *Controlled Bi-directional Quantum Teleportation of Superposed Coherent State Using Five Qubit Cluster-type Entangled Coherent State as a Resource* (2021). arXiv:2105.
44. Yuan, H., Liu, X. Y. & Zhang, Z. J. Bidirectional quantum operation teleportation with two four-qubit cluster states. *Quantum Inf. Process.***23**(4) (2024).
45. Chiribella, G., D'Ariano, G. M. & Perinotti, P. Theoretical framework for quantum networks. *Phys. Rev. A* **80**, 022339 (2009).
46. Buluta, I. & Nori, F. Quantum simulators. *Science* **326**, 108–111 (2009).
47. Wang, L., Niu, Q., & Fei, M. A novel quantum ant colony optimization algorithm. In *International Conference on Life System Modeling and Simulation*. (Springer, Berlin, Heidelberg, 2007).
48. Waxman, B. M. Routing of multipoint connections. *IEEE J. Sel. Areas Commun.* **6**, 1617–1622 (1988).

Acknowledgements

This paper is derived from a research grant funded by the Research, Development, and Innovation Authority (RDIA)- Kingdom of Saudi Arabia - with grant number (13325-psu-2023-PSNU-R-3-1-EF). Also, the authors would like to thank Prince Sultan University for their support.

Author contributions

NI: Writing – original draft, Investigation, Software, Formal analysis, Data curation. PK: Writing – original draft, Investigation, Software, Formal analysis, Data curation. AS: Writing – review & editing, Visualization, Validation, Supervision, Project administration, Methodology, Investigation, Conceptualization. BK: Writing – review & editing, Visualization, Validation, Supervision, Project administration, Methodology, Investigation, Conceptualization. RAL: Supervision, Review & editing. MZ: Review & editing. AAA: Review & editing.

Funding

The Research, Development, and Innovation Authority (RDIA)- Kingdom of Saudi Arabia - with grant number (13325-psu-2023-PSNU-R-3-1-EF).

Declarations

Competing interests
The authors declare no competing interests.

Additional information
Correspondence and requests for materials should be addressed to A.S.

Reprints and permissions information is available at www.nature.com/reprints.

Publisher's note Springer Nature remains neutral with regard to jurisdictional claims in published maps and institutional affiliations.